Behavioral Evaluation of Small-Diameter Defective and Intact Bored Piles Subjected to Axial Compression

P.J.R. Albuquerque, J.R. Garcia, O. Freitas Neto, R.P. Cunha, O.F. Santos Junior

Abstract. Foundation engineering has continually sought to understand the behavior of piles subjected to loads and their influence on the overall structural behavior. Recently, more load tests are being performed in construction due to the recommendations of the NBR6122/2010 Brazilian code. The available literature offers few reports on pile behavior in a faulty foundation. Therefore, the present study assessed the behavior of a single pile with and without a defect: 5 m long, small-diameter ($\phi = 0.25$ m) bored piles were embedded in diabase soil (porous, lateritic and unsaturated) at Experimental Site II (Unicamp). The piles behavior were compared by laboratory tests, numerical analysis using the finite element software LCPC Cesar v.4.07 and experimental results from slow maintained load (SML) tests. Strain gauge instruments were installed at the top and tip of each pile. As predicted by the numerical analyses, when subjected to the first stage of the pile load test, the defective region of the pile failed structurally; however, the pile was still able to resist or "absorb" loading. Factors related to the loading ratio of the foundation, the total and differential displacements and the rotation of the top block were examined. The results obtained in the two analyses (numerical and in situ) were satisfactory and showed significant agreement, providing greater understanding of the complex behavior of this foundation system.

Keywords: defective pile, bored pile, load test, instrumented piles

1. Introduction

One of the main topics of study in foundation engineering is the load capacity of a structural element embedded in the ground. Theoretical and semi-empirical methods are used to calculate the bearing capacity, and refined numerical tools are used to predict foundation behavior. However, the most reliable method for analyzing the bearing capacity and foundation behavior is to conduct load tests, that reduce the uncertainties and provide greater savings to the project. If none of the construction site piles experience installation problems, such as failures during the installation, use of low quality materials or poor performance evaluation, the project risk decreases. However, the risk may increase if some foundation piles have a defect that could compromise the load capacity of the pile group.

In addition to the interactions predicted by the relevant calculations and design methodologies, the behavior of a single pile-top block system with a defective pile was evaluated in this study. A pile defect can be considered to be a "hidden variable" from an analytical point of view because it is not included in the design. Therefore, in the general context, defects appear as a result of unknown uncertainties or negligence in installation. In addition to the technical difficulty of addressing such a problem, studies on this subject are faced with a lack of data and available information from the pile manufacturers and installers.

Several studies have been conducted on blocks with defective piles; however, these studies are exclusively theoretical, numerical or associated with experiments on reduced-scale models. Among the most significant studies are those of Makarchian & Poulos (1994), Abdrabbo (1997), Xu (2000), Prakoso & Kulhawy (2001), Petek *et al.* (2002), Kong & Zhang (2004), Novak *et al.* (2005), Zhang & Wong (2007), Cordeiro (2007), Cunha *et al.* (2007), Cunha *et al.* (2010), Chung *et al.* (2010), Leung *et al.* (2010), Omeman (2012) and Freitas Neto *et al.* (2013). Full-scale experimental studies are rare, especially those including pile defects.

Considering the lack of information available in the literature and the relevance of this subject, the present study assessed the behavior of a full-scale foundation with and without defective piles. The defective foundation element was sized and analyzed in the laboratory before it was installed and loaded in the field. The piles were installed at Experimental Site II of the University of Campinas (Universidade Estadual de Campinas – Unicamp). They were subjected to a slow maintained load (SML) test: intact pile (Garcia, 2015) and defective pile (Freitas Neto, 2013).

Paulo José Rocha de Albuquerque, Ph.D., Associate Professor, Faculdade de Engenharia Civil, Arquitetura e Urbanismo. Universidade Estadual de Campinas, Campinas, SP, Brazil. e-mail: pjra@fec.unicamp.br.
Jean Rodrigo Garcia, Ph.D., Associate Professor, Faculdade de Engenharia Civil, Universidade Federal de Uberlândia, Uberlândia, MG, Brazil. e-mail: jean.garcia@ufu.br.
Osvaldo Freitas Neto, Ph.D., Associate Professor, Departamento de Engenharia Civil, Universidade Federal do Rio Grande do Norte, Natal, RN, Brazil, e-mail: osvaldocivil@ct.ufrn.br.
Renato Pinto da Cunha, Ph.D., Associate Professor, Universidade de Brasília, Brasília, DF, Brazil. e-mail: rpcunha@unb.br.
Olavo Francisco dos Santos Junior, Ph.D., Full Professor, Departamento de Engenharia Civil, Universidade Federal do Rio Grande do Norte, Natal, RN, Brazil. e-mail: olavo@ct.ufrn.br.
Submitted on October 8, 2016; Final Acceptance on May 5, 2017; Discussion open until December 29, 2017.

2. Pile Foundation Pathologies

Pile defects may be of structural and/or geotechnical origin. Geotechnical defects arise due to problems resulting from poorly conceived projects, poor geological-geotechnical characterization and improper pile installation. The most commonly cited geotechnical problems are those associated with lower than expected tip and lateral bearing capacity due to, for example, the presence of compressible and low resistance soil layers (Poulos, 2005).

Structural bearing capacity, manufacturing and installation problems that affect pile performance are mainly due to discrepancies in size, concrete strength and other variables between the design values and the actual values on site (Poulos, 1997). These defects typically manifest as a sharp reduction in the pile cross section due to necking of cracked sections and damaged areas on the pile.

In the case of bored piles, the most common problems are low cement content in concrete mass, inappropriate mixing and inadequate pouring, which results in concrete segregation and setting delays. The collapse of unprotected excavation walls during concreting and a lack of pile continuity can result in a reduced cross section area, which compromises the pile performance.

Statistical data about pile defects are scarce and have rarely been published. Klingmüller & Kirsch (2004) presented a German study of low-strain pile integrity testing to analyze cast-in-place piles. The authors showed that 15% of the tested piles presented results that caused concern, while 5% indicated very clear problems that required intervention. The authors also mentioned that 30% of the defective piles presented poor concrete, 21% showed insufficient length, *i.e.*, the piles were shorter than predicted in design, 14% showed shaft strangulation (necking) and 35% showed problems related to structural cracking. According to these authors, 18% of pile integrity verification tests are usually performed due to suspicion of failure, 26% on grounds that present "special" behavior and 56% as part of routine checks.

This paper analyzes the effects of necking and the use of a low quality concrete in the same pile section and their influence on the foundation performance.

3. Experimental Area

The Unicamp Experimental Site II, is located close to the School of Civil Engineering, Architecture and Urban Design at Unicamp, in Campinas-SP, Brazil, in a region that includes the basic intrusive rocks of the Serra Geral Formation (Diabase) of the São Bento Group. Pedologically, soils of this region can be classified as purple latosols, mineralogically consisting of quartz, ilmenite, magnetite, kaolinite, gibbsite, iron oxides and hydroxides; this typical layer of soil may have a thickness ranging from 5 to 30 m (Zuquete, 1987), with an unsaturated, porous and collapsible upper zone close to the surface. Figure 1 shows the simplified geological-geotechnical profile of the experimental site obtained from laboratory tests performed by Gon (2011) as well as from standard penetration tests (SPTs) and cone penetration tests (CPTs) conducted by Rodriguez (2013).

4. Methodology

The objective of this study was to evaluate the behavior of a bored pile with and without a defect based on experiments and numerical analysis using the finite element method (FEM). In both the numerical analysis and experimental SML tests, information was obtained regarding the load capacity of the foundation, the total and differential settlements, and the rotation of the block as well as the load distribution along the pile shaft and at the pile tip.

4.1. Numerical analyses

Numerical analyses were performed using the LCPC-CESAR v.4.07 software, developed at the *Laboratoire Central des Ponts et Chaussées* (Road and Public Works Research Institute). This software is a 3D FEM (Finite Element Method) tool. To adequately balance the computational effort and the convergence of the obtained results, a quadratic pentahedral element consisting of 15 nodes was used.

The FEM program was useful in predicting the load *vs.* displacement behavior and the load transfer along the pile shaft. To ensure the reliability of the numerical analysis results, three verifications were performed before initiating the analyses:

a) Comparison with available published results;
b) A convergence test to ensure that the boundary conditions did not influence the analysis results; and
c) Comparison of the soil parameters used in the analysis with the experimental results.

A convergence test, which consists of verifying whether the boundary conditions provide results that are in accordance with the pre-established definitions, was performed in the preprocessing step to validate the half-space dimensions, *i.e.*, the model geometry. Comparisons with available results were made to ensure the applicability of the program to the problems addressed in this study.

After completing the steps outlined above, the finite element model was calibrated by comparing the results of a load test on a single pile (L = 5 m and ϕ = 0.25 m) that was evaluated by Schulze (2013) at the FEC-Unicamp experimental site for the same pile, using the properly adjusted soil parameters that were originally obtained by Gon (2011). The Mohr-Coulomb constitutive model was considered adequate for the soil behavior. The parabolic plastic model, which is available in the LCPC-CESAR v.4.07 software, was used for the concrete.

The numerical analyses performed in this study were subdivided into two stages. The first stage was the calibration of the geotechnical parameters in the Mohr-Coulomb

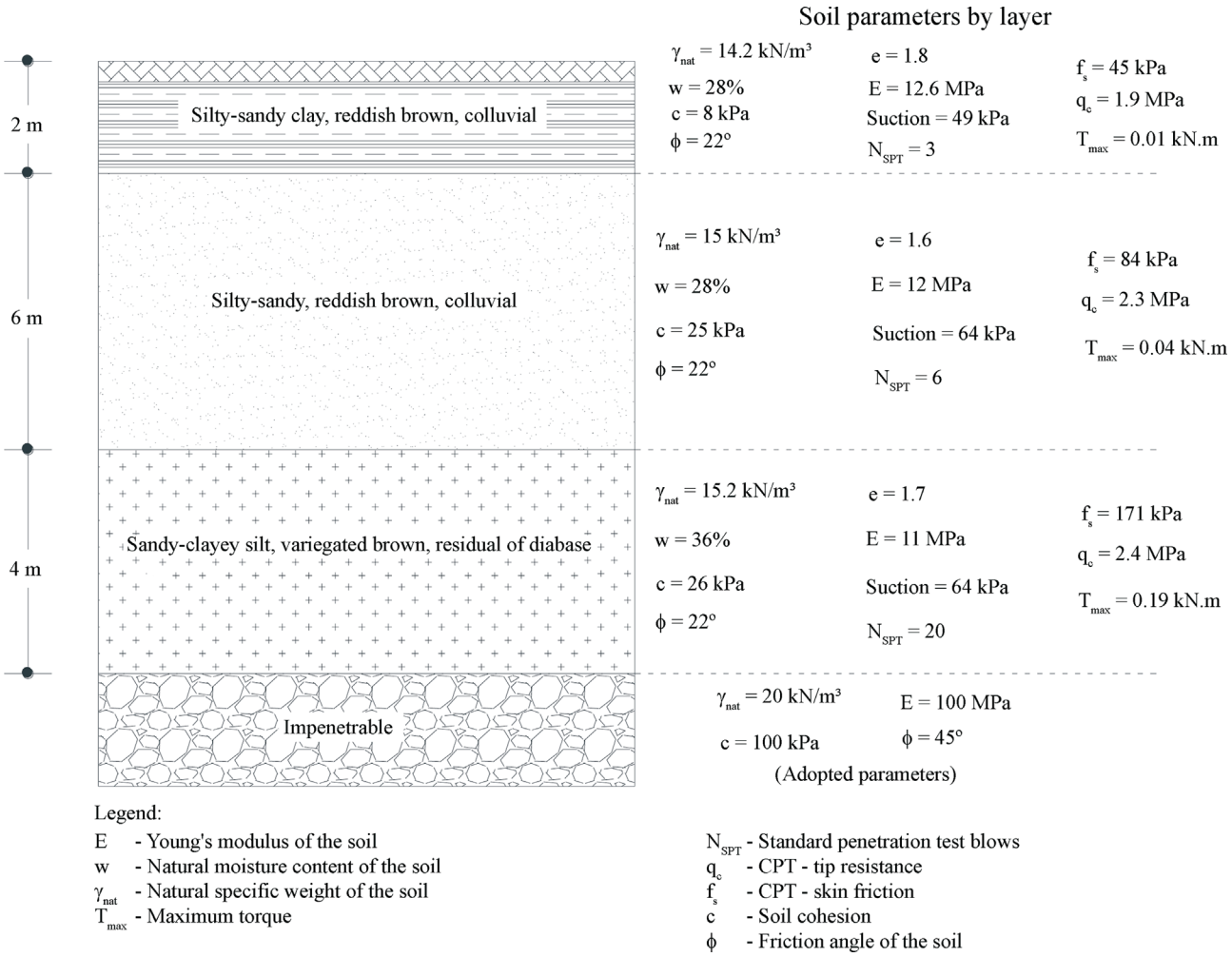

Figure 1 - Average parameters of the geological profile at the experimental site (Garcia, 2015).

constitutive model and the subsequent acquisition of the parameters used for the design and modeling of the defective pile area. The second stage a comprised numerical analysis of the intact pile.

4.1.1. Calibration of geotechnical parameters and the defect size

The numerical analysis showed that the geotechnical parameters obtained by Gon (2011) presented similar behavior to those obtained experimentally by Scallet (2011) and Schulze (2013) in load tests on isolated piles. Because these piles have the same geometric characteristics and the tests were performed in the same experimental field as those in the present study, the same geotechnical parameters obtained by Gon (2011) were used in all of the numerical analyses in this paper.

Several criteria were used to determine the conventional ultimate load. In this study, the criteria used to determine the conventional ultimate load were those from Décourt (1993), Décourt (1995) and the British Standard (BS 8004:2015), which indicates that the conventional ultimate load for precast and bored piles must be equivalent to a load corresponding to a settlement of nearly 10% of the nominal pile diameter. When applying this criterion to the load *vs.* displacement curves obtained by Scallet (2011) and those from Schulze (2013), the conventional ultimate loads were approximately 150 kN and 175 kN, respectively, at a displacement of 10% of the pile diameter, *i.e.*, 0.025 m.

The conventional ultimate load in the FEM numerical analysis conducted by Freitas Neto (2013) was approximately 163 kN. For that load at the pile head, the load ranged from 130 kN to 140 kN close to the faulty section, which occurred at a depth of 1.9 m and 2.5 m, respectively. Therefore, the average geotechnical ultimate load corresponding to the cross section with a defect was 135 kN. Thus, when applying a safety factor of two (2.0), an allowable structural load of approximately 68 kN was obtained. Thus, 68 kN was assumed to correspond to the load at which the defective zone of the pile would be compromised when subjected to an axial load in the field.

After determining the axial load under which the cross section would present a poor performance when sub-

jected to loading, the defective section of the pile was modeled in the laboratory to simulate a structural defect on the pile. The defective section of the pile was molded with mortar at a cement-to-sand ratio of 1:9 and a water-to-cement ratio of 1.50. The intact cross section of the pile measured 25 cm in diameter; however, to simulate a reduction in the cross section, a hollow cylinder with an equivalent diameter of 18.4 cm was molded, *i.e.*, the cross section of the intact pile was decreased by 26.4%. Specimens with a diameter of 0.25 m and a height of 0.60 m, simulating the cross section of the pile, were subjected to compressive strength tests in the laboratory at full-scale.

4.1.2. Numerical analysis of the intact and defective piles

To obtain the parameters used to compare the foundations with and without defective piles, numerical analyses were performed on respective blocks with the intact and defective piles. Table 1 and Fig. 2 show the geometric characteristics used in the numerical analysis performed in this study, while Table 2 presents the material parameters used in the numerical analyses.

4.2. Pile construction and static load tests

Figure 3 shows the cross section and dimensions of the piles under the block as well as the dimensions and position of the defect. This figure also shows the positions of the instrumentation, with strain gauges installed at the top and tip of the pile.

Two bored test piles were constructed with lengths of 5 m and diameters of 0.25 m. The intact pile was fully reinforced along its shaft with four CA-50A steel bars (ϕ = 10 mm) and spiral stirrups of CA-50 steel (ϕ = 6.3 mm). In the defective pile, the longitudinal reinforcement was divided into two segments of 2.5 m, and a segment of 0.6 m was removed from the upper half of the reinforcement. This stirrup section removed from the reinforcement corresponds to the position of the defect.

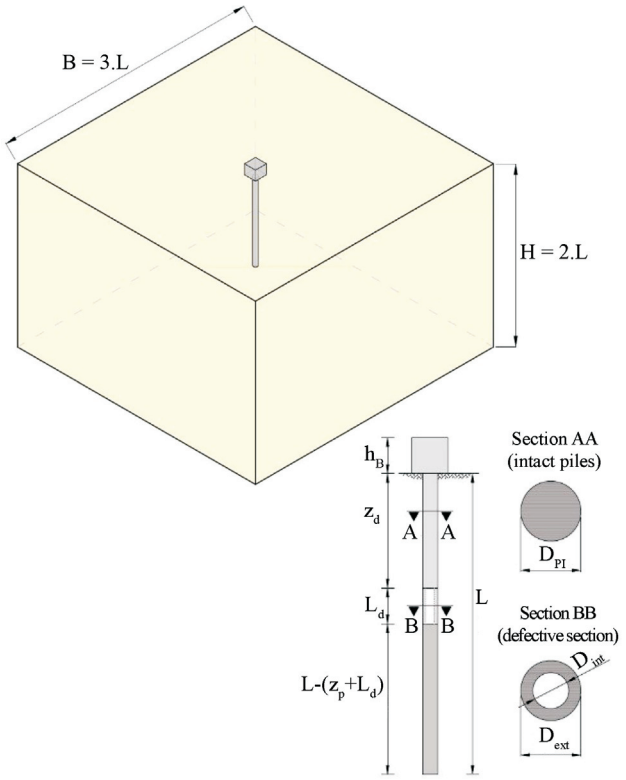

Figure 2 - Detail of the geometric dimensions (numerical analysis).

The construction sequence of the defective pile was as follows: positioning the reinforcement for the lower section at the bottom of the bored hole, pouring concrete in the lower 2.5 m section of the pile, installing the precast hollow cylinder mortar to form the defect on top of the poured concrete (with sealed ends on the cylinder), installing the reinforcement of the upper section of the pile and final pouring of concrete (Fig. 4).

Table 1 - Geometric dimensions.

D_{PI} (m)	D_{PD} (m)	A_{PI} (m^2)	A_{PD} (m^2)	B (m)	L (m)	L_d (m)	z_d (m)	H (m)	s/D_{PI}
0.25	0.185	0.049	0.027	15	5.0	0.60	1.90	10	5.0

D_{PI} – Diameter of the intact piles; D_{PD} – Equivalent diameter of the defective pile cross sections; A_{PI} – Area of the intact cross section of the piles; A_{PD} – Area of the defective cross section of the piles; B – Horizontal dimension; L – Length of the pile; L_d – Length of the defective zone; z_d – Depth of the defect; H – Vertical dimension; and s/D_{PI} – Relative spacing.

Table 2 - Material properties.

$E_P = E_R$ (GPa)	E_{PD} (GPa)	E_S (MPa)	ν_c	ν_S	f_{ck} (MPa)	f_{ct} (MPa)
28.5	5.9	Figure 1	0.20	0.45	25	2.5

$E_P = E_R$ – Young's modulus of the concrete piles; E_{PD} – Young's modulus of the defective material; ν_c – Poisson's ratio of the concrete; ν_s – Poisson's ratio of the soil; f_{ck} – Compressive characteristic strength of the concrete; f_{ct} – Tensile characteristic strength of the concrete.

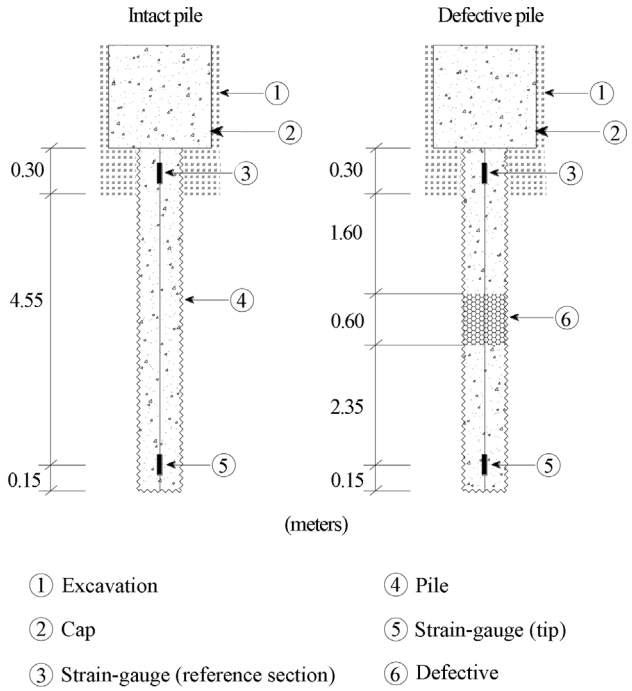

Figure 3 - Positions of the instrumentation and the Defect.

Instrumentation on the pile was placed along the reinforcement axis at the top and tip of the pile. Furthermore, before positioning the block reinforcement, the instrumentation wires were properly protected by running them through PVC tubes.

4.3. Load tests

SML tests were conducted according to the NBR 12.131 (ABNT, 2006) procedure. The reaction scheme consisted of bored piles ($\phi = 0.6$ m and $L = 9.0$ m) that were designed to resist the tensile stresses caused by the reaction system during the load tests. The piles were reinforced with 10 CA-50 steel bars (ϕ = 10 mm) and CA-50 steel spiral stirrups (ϕ = 6.3 mm). This reinforcement was completed by installing a Dywidag tie rod with a 9.2 m length and diameter of 32 mm. The reaction beam used in the load tests was 5.3 m long and was formed by the union of two I-beams capable of resisting up to 2 MN (Fig. 5).

A load cell with a maximum capacity of 2 MN was used for the load measurement at the top block. Displacement readings were obtained via four displacement transducers with a range of 100 mm.

5. Results and Discussion

This section presents and discusses the results of foundation blocks on an intact single pile and a defective single pile obtained experimentally ($SD_{1(EXP)}$ and $CD_{1(EXP)}$) from two static load tests and the results obtained numerically from three-dimensional finite element modeling with the LCPC-CESAR software ($SD_{1(NUM)}$ and $CD_{1(NUM)}$). Further-

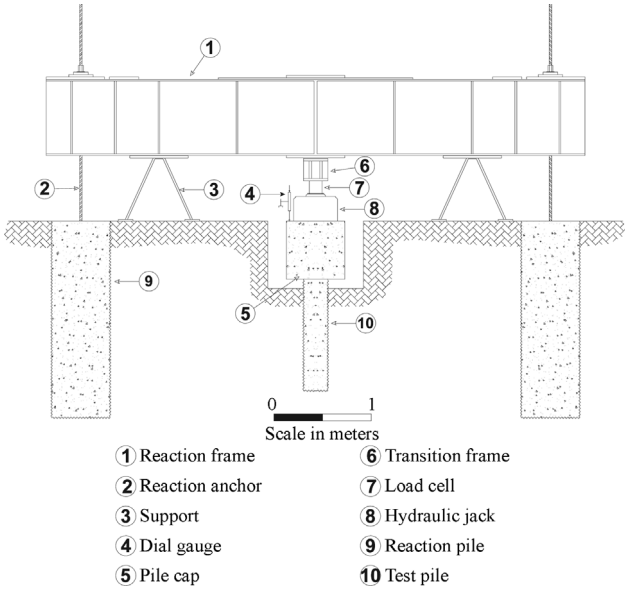

Figure 5 - Front view sketch of the main reaction system (Garcia, 2015).

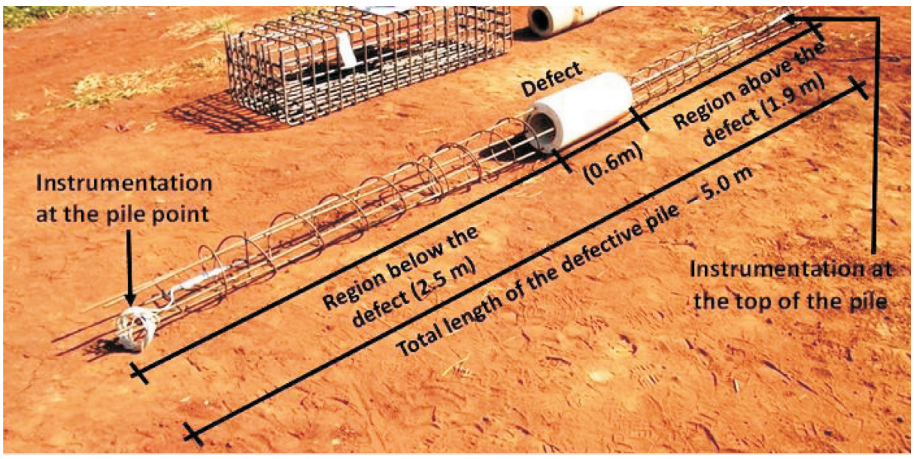

Figure 4 - Longitudinal diagram of the defective pile (Freitas Neto, 2013).

more, the behavior associated with the loading and displacement is discussed along with the load distribution between the block and the pile before and after structural failure.

5.1. Load *vs.* displacement curve

This section presents the results obtained experimentally and numerically for top loading the piles as well as analyses referring to the ratio between the applied load and the conventional ultimate load (Q/Q_{ult}) associated with top loading. Figure 6 correlates the load *vs.* displacement curves obtained numerically and experimentally. These curves show that the conventional ultimate loads were defined for 25 mm of settlement (10% of the nominal pile diameter). The curves in Fig. 6 clearly show that the experimental and numerical curves of the piles without defects exhibit similar behavior up to 50% of the ultimate load (1/2 Q_{ult}); after this point, the experimental curve showed less displacement for the same load. For the defective pile, different behavior was noted from the start of loading. The experimental curve for the defective pile was unaltered for low load values applied on top of the block (Q < 60 kN). The displacements of the curve obtained from numerical simulation were higher than those observed experimentally; however, the experimental curve showed a sudden failure at 100 kN, while the results from the numerical simulation indicated that the pile continued to absorb load after this point.

Table 3 summarizes the conventional ultimate load values, the total displacement and maximum and average differential displacement obtained from both the numerical analysis and the static load test performed in the field.

Using the data in Table 3, an additional analysis was conducted using the ratio between the applied and ultimate load (Q/Q_{ult}) both numerically and experimentally. Figures 7 and 8 present these results in terms of the intact and the

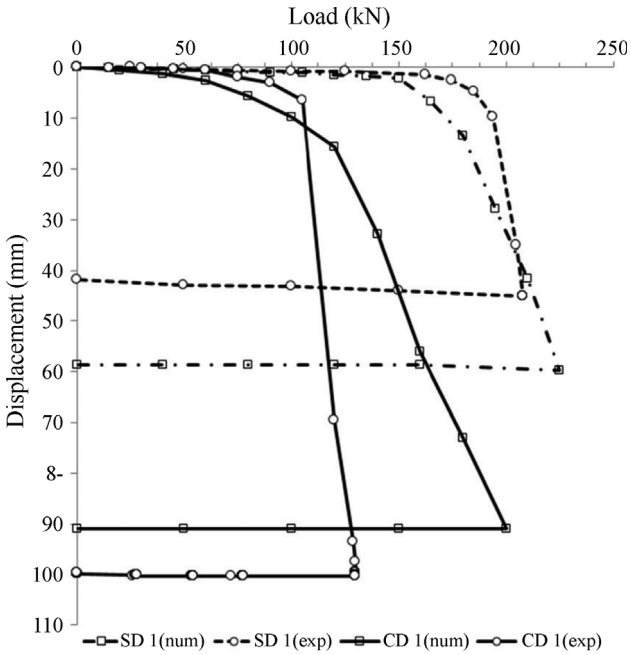

Figure 6 - Load *vs.* displacement curve.

Table 3 - Results obtained from the load test and numerical simulations.

Pile	ΔQ (kN)	Q_{ULT} (kN)	$\rho_{10\%D}$ (mm)	ρ_{MMAX} (mm)
$SD_{1(NUM)}$	15	225	25	59.8
$SD_{1(EXP)}$	15	208	25	45.1
$CD_{1(NUM)}$	20	200	25	91.0
$CD_{1(EXP)}$	15	130	25	~ 100.0

ΔQ – Load increase applied in each loading stage; Q_{RUPT} – Geotechnical ultimate load of the foundation; $\rho_{10\%D}$ – Displacement for a settlement of 10%D; and ρ_{MMAX} – Maximum displacement at the end of loading.

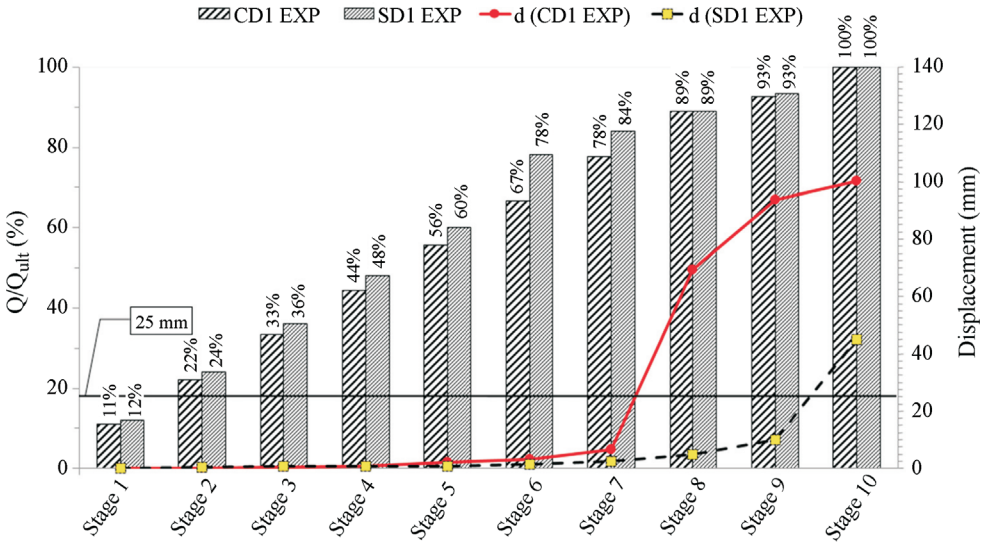

Figure 7 - Graph of the Q/Q_{ult} and displacement (experimental).

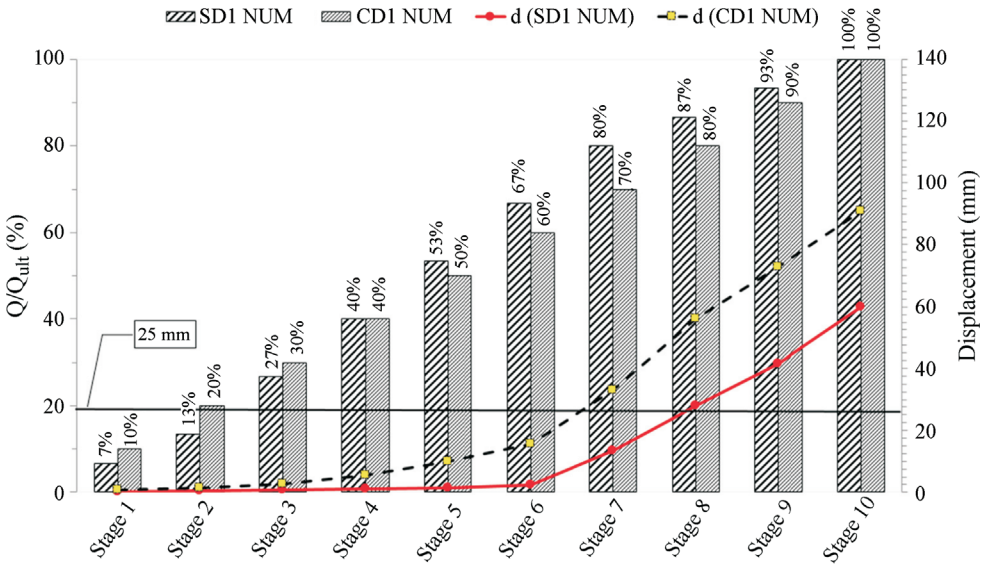

Figure 8 - Graph of the Q/Q_{ult} and displacement (numerical).

defective piles. For the defective pile, the experimental displacement was less than 5 mm up to the 7th stage (approximately 80% of the ultimate load), after which it abruptly increased to +80 mm at the ultimate load. In contrast, the displacement remained less than 10 mm up to the 9th stage for the intact pile. In both cases in the numerical simulations, the displacements remained low and approximately constant up to the 5th stage (120 kN). After that point, the defective pile sharply increased its displacement up to +80 mm at the ultimate load (200 kN), with similar behavior (but at a lower degree) for the intact pile.

The above results clearly indicate that the defective pile indeed failed earlier than expected: the experimental ultimate load of the intact pile (208 kN) was 43% higher than the equivalent ultimate load for the defective pile (135 kN). The Q/Q_{ult} ratio was also higher for the intact pile than for the defective one at the 25 mm displacement level. In terms of the final displacement at the ultimate load, it is clear that for any of the studied cases, the intact pile had a much smaller final displacement than the defective one. Directly comparing both the load and displacement results clearly indicate the contrasting characteristics of the defective and intact piles.

Figures 9 and 10 present the experimental results and the numerical results for the intact and defective piles, respectively.

Figure 9 shows the Q/Q_{ult} ratio for the intact pile obtained both numerically and experimentally. This figure shows that the displacements were similar up to the 6th stage, which represents approximately 70% of the ultimate

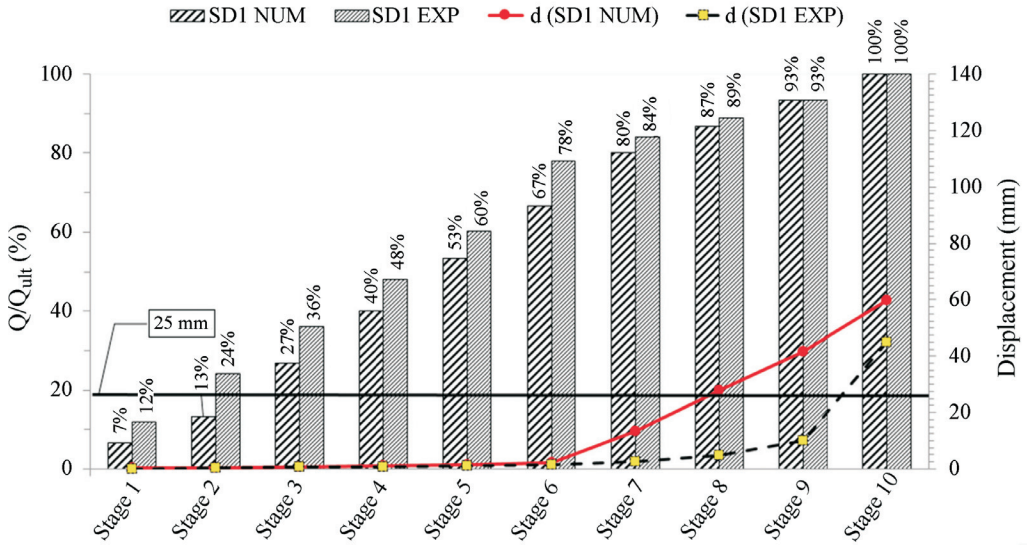

Figure 9 - Graph of the Q/Q_{ult} and displacement determined numerically and experimentally (intact pile).

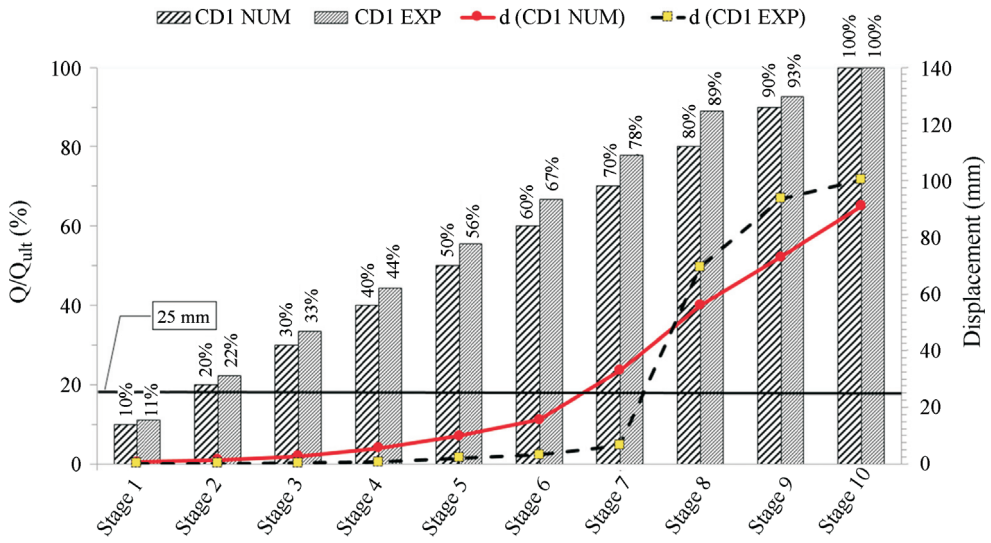

Figure 10 - Graph of the Q/Q_{ult} and displacement determined numerically and experimentally (defective pile).

load. After this point, the experimental displacements were consistently lower than those obtained numerically. At the ultimate load (10th stage), the differences between the numerical and experimental displacements sharply decreased, although the numerical value was approximately +30% higher than the experimental value. At the 25 mm reference displacement, both the numerical and experimental loads were approximately similar; however, the Q/Q_{ult} ratio differed drastically (95% for the experimental case compared to 87% for the numerical case).

Figure 10 expands the analysis for the defective pile; this figure illustrates that the defective pile showed distinct behavior (compared to the previous figure) when comparing the numerical and experimental results. At the 25 mm reference displacement, the numerical and experimental loads were quite different (65% of the ultimate load for the numerical case and 78% for the experimental case). Moreover, for the same Q/Q_{ult} (> 80%), unlike Fig. 9, the experimental displacements were consistently larger than the numerical values.

5.2. Tip and lateral loads

This section analyzes the data related to the load transfer along the depth and the mobilized skin friction. Figures 11 and 12 present the graphs of the average axial load transfer in the piles along their depth as obtained in the load tests. The axial load on the piles was assumed to vary linearly with depth, and the presented loads correspond to those obtained directly at the top of the piles. Mobilization of skin friction occurs from the 1st to 6th stage coupled with a small participation of tip resistance. Skin friction depletion occurs after the 6th stage, as evidenced by the parallel straight lines, concurrent with the mobilization of tip resistance, registering the maximum value of this resistance in the 11th stage (208 kN). Figure 12 shows the load distribution for the defective pile, indicating that the tip resistance

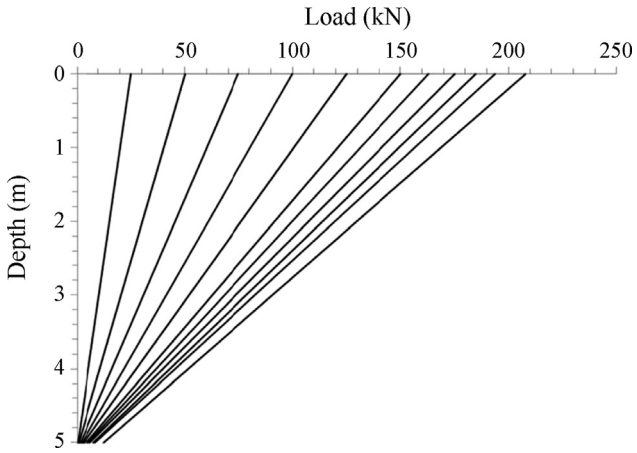

Figure 11 - Load transfer in the intact pile (experimental) (Garcia, 2015).

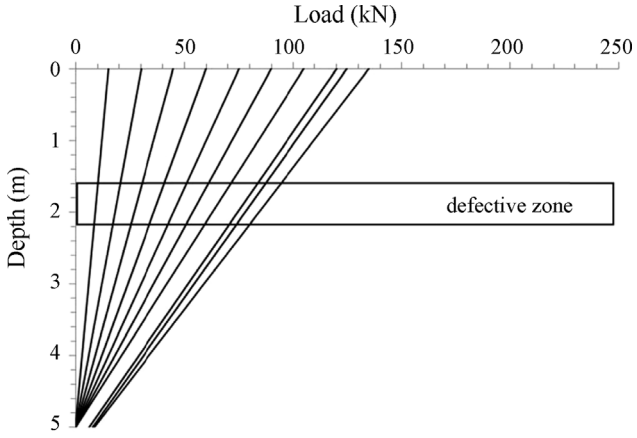

Figure 12 - Load transfer in the defective pile (experimental) (Freitas Neto, 2013).

was mobilized after the 7th stage (105 kN); from this point on, a depletion of skin friction was observed, as verified by the parallel straight lines of the load transfer. The defective pile structurally failed when its internal load reached a level close to 105 kN, and naturally, from this point on, there was no proportionality anymore between applied load on top of the pile and measured load on its tip. Nevertheless (and surprisingly), the defective pile did continue to "absorb" applied loads from the block, beyond its structural failure, indicating that even "failed" it continued somehow to accomplish its primary function of receiving and delivering superstructure loads to underlying more competent soil layers.

Figures 13 and 14 show the load distribution along the depth obtained from the numerical analysis. For the intact pile, the tip load was mobilized from the start of loading but at a low magnitude. Similarly, the defective pile presented lower tip mobilization than that obtained for the intact pile.

Figures 15 and 16 presents the total load at the top and lateral loads *vs.* displacement obtained from the load tests and the numerical models. Skin friction was responsible for most of the load absorbed by the piles. For the values obtained experimentally, small displacements were required for complete mobilization of skin friction, maintaining the tendency for friction stabilization after its depletion (Fig. 15). This phenomenon was not observed in the numerically obtained results; the lateral load did not present a clear definition of depletion, considering the load increase

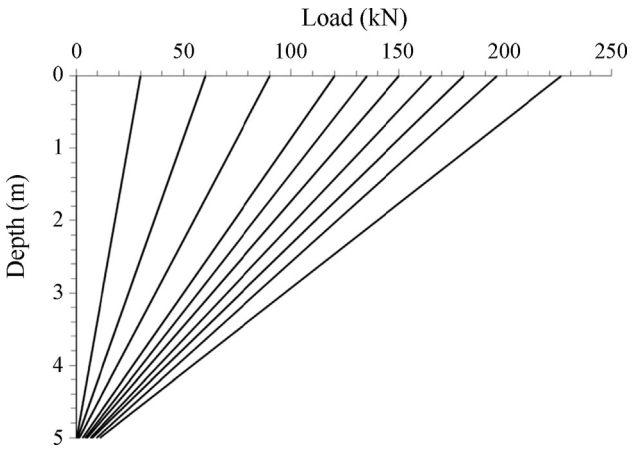

Figure 13 - Load transfer in the intact pile (numerical) (Freitas Neto, 2013).

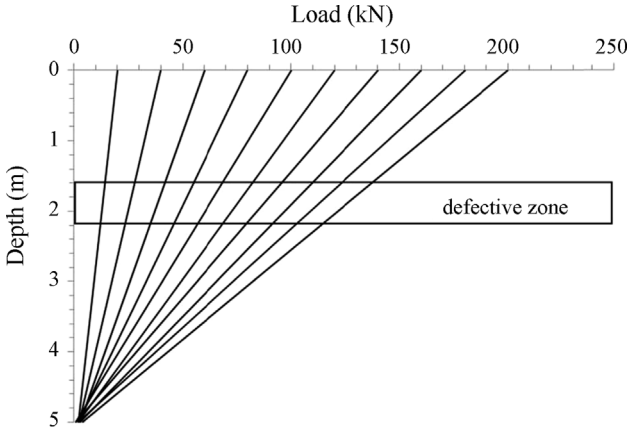

Figure 14 - Load transfer in the defective pile (numerical) (Freitas Neto, 2013).

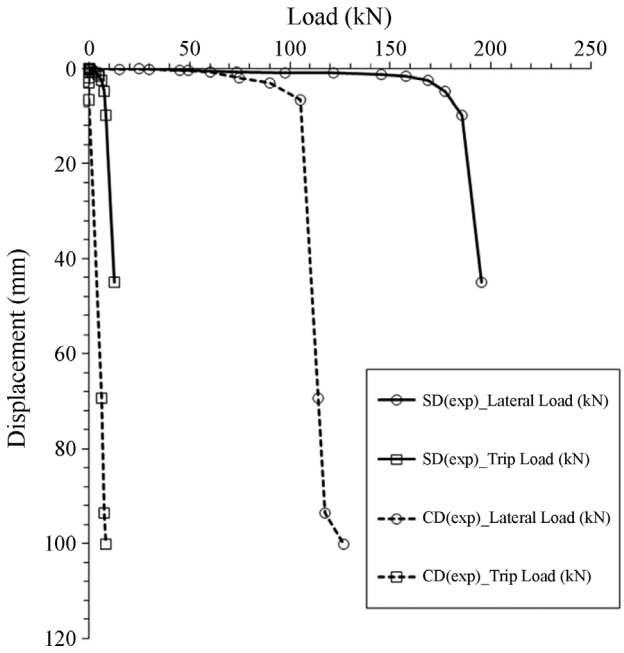

Figure 15 - Curves of top and lateral loads *vs.* displacement (experimental).

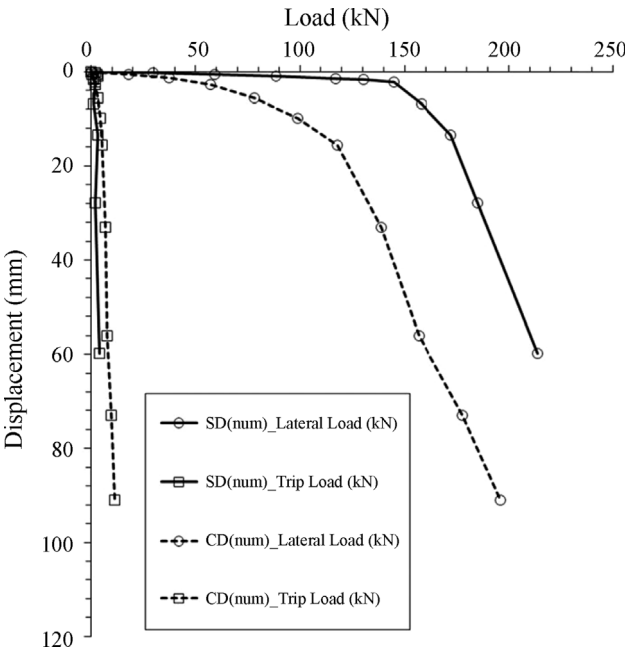

Figure 16 - Curves of top and lateral loads *vs.* displacement (numerical).

after the inflection point in the lateral load *vs.* displacement graph (Fig. 16).

For the intact pile, the skin friction at the maximum load of the load test (208 kN) was on the order of 50 kPa (Fig. 15). This value is close to the value obtained by Albuquerque (2001) from instrumented load tests on bored piles at Experimental Field I – Unicamp, which is close to the location of the tests in this study. For the defective pile, the skin friction for the maximum load (135 kN) was approximately 32 kPa. This value is 36% lower than that obtained for the intact pile. However, observing the friction value of the intact pile associated with the ultimate load of the defective pile (135 kN), the value was approximately 31 kPa. This result indicates that before the defect manifests, the friction of the defective pile is very similar to that of the intact pile.

The same skin friction trend was observed in the numerical analysis for both ultimate loads (Q_{ult}) and working (half of ultimate) loads ($Q_{ult/2}$), indicating that the modeling results were similar to the experimental data (Figs. 17 and 18).

5.3. Evaluation of differential displacements at the top of the defective pile

This section analyzes the influence of the defect on the behavior at the top of the pile during the loading tests. The differential displacements obtained experimentally may be due to a potential eccentricity of the faulty pile, *i.e.*, the construction and interference of the defect resulted in the imbalance of the pile/block assembly because it was not laterally confined. Figure 19 shows the settlement values recorded by each of the linear variable differential transformers (LVDTs). The maximum settlements were registered by LVDT 1 and LVDT 2. The maximum differential settlement recorded at the end of the load test on this block was 25.6 mm between LVDTs 1 and 3.

Figure 19 shows the values of angular rotation on top of the block for each level of applied load. This figure dem-

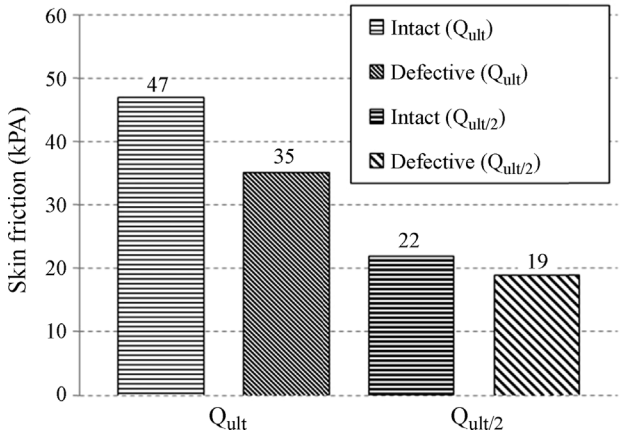

Figure 17 - Graph of skin friction (experimental).

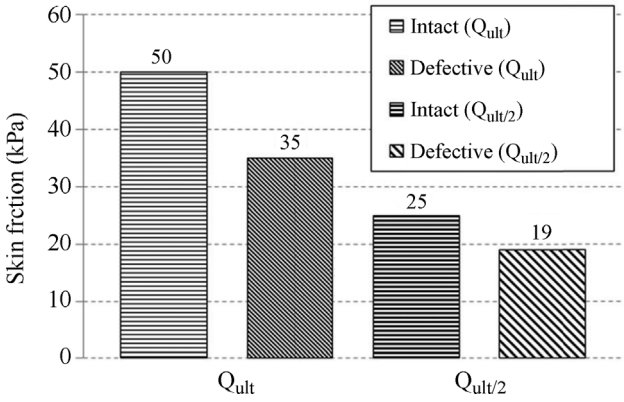

Figure 18 - Graph of skin friction (numerical).

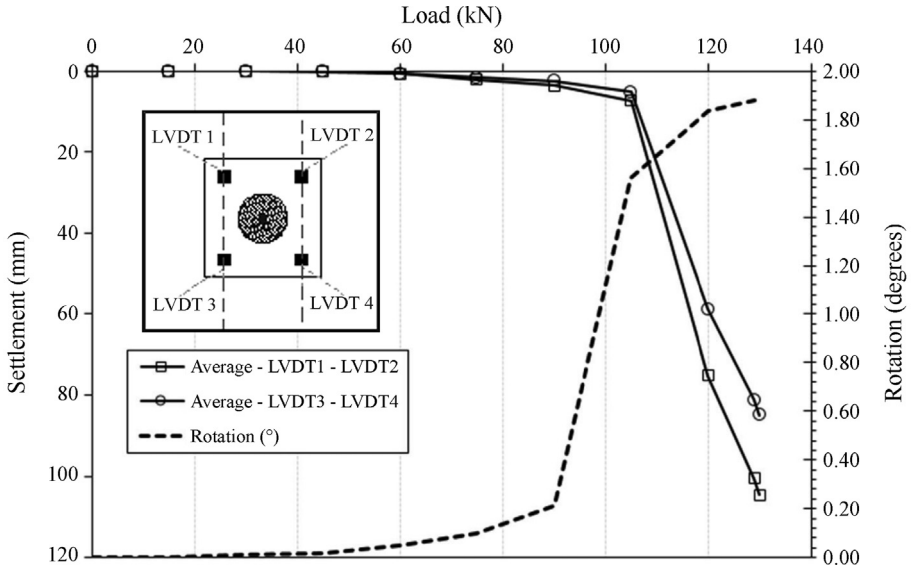

Figure 19 - Block rotation and average settlement with each load increase (CD 1).

onstrates that the $CD_{1(EXP)}$ pile began to exhibit significant rotations after 60 kN of applied load, reaching approximately 1.9º when approaching the conventional ultimate load stage (110 kN). In absolute terms, this rotation angle is equivalent to a vertical displacement in the order of 20 mm at the extremities of the top block. So, besides bearing capacity concerns on the design of the foundation, excessive differential settlements (*i.e.*, rotations) seem to be the major design issue when having defective piles in a vertically loaded deep foundation.

5.4. Evaluation of the defect (*in situ*)

After conducting the load tests, a 3.0 m deep and 0.90 m in diameter excavation was dug adjacent to the defective pile to verify whether the defective cross section of the pile had failed after the loading test. Figures 20 and 21 show the success in predicting the behavior of the defective pile region; the defect was in fact mobilized when the load tests were performed. The failure mode of the defective zone of the pile was similar in the laboratory (Fig. 22) and in the field.

6. Conclusions

Based on the results and analyses, the following conclusions were made:

- The load tests performed on the piles with and without a defect showed varying behaviors when subjected to different loads. The defect was responsible for an approximately 50% reduction in the ultimate load. This result proves, as expected, that a defect in the pile may compromise the stability of a group of piles, thus demonstrating the need to identify anomalies in piles.
- The pile defect was located at approximately 1.9 m below the block and clearly influenced the load capacity of the pile and therefore affected the rotation of the pile block system. This behavior would perhaps differ if the defect was located at another section or depth, although

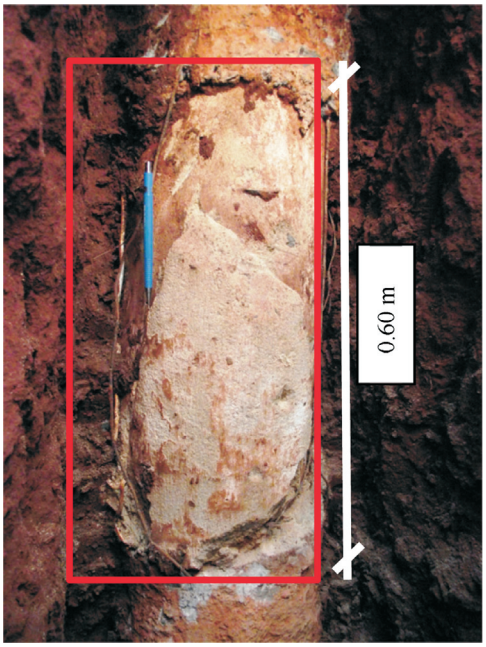

Figure 20 - Defective zone of the pile mobilized after performing the load test on block $CD_{1(EXP)}$.

Figure 21 - Detail of the defect after performing the load test on block $CD_{1(EXP)}$.

Figure 22 - Sample after failure stage (laboratory test).

this was not tested in this study. In this case, the defect would be expected to have less influence on the system behavior if it was located closer to the pile's tip. However, more research is needed on this topic.

- The results obtained from numerical modeling using the LCPC-Cesar v.4.07 software with the geotechnical parameters determined by Gon (2011) satisfactorily predicted the behavior of the piles with and without a defect. The difference with respect to the experimental data was related to the behavior of the load *vs.* settlement curve. The numerical analyses presented higher displacements than the experimental results for the same load.
- Foundations are designed according to the load obtained after applying a safety factor of two (working load), which generally corresponds to half of the ultimate load of an intact foundation. For the intact pile, the working load was equivalent to 85 kN, exceeding the 55 kN working load of the defective pile. Therefore, it is important to highlight the significant rotation at the top of the pile, even if it is almost equivalent to the working load of the foundation. If this pile was designed for loads equivalent to the working load (85 kN), it would probably not fail during the foundation's lifetime but would probably suffer excessive total and differential settlements.
- In general, the piles worked mainly through skin friction, which was responsible for approximately 95% of the load applied to the top. This result was indeed expected for the bored piles installed in this type of soil (porous, laterite and unsaturated). The friction values obtained both numerically and experimentally were similar, indicating that the numerical model provided satisfactory results.
- The load friction of the piles obtained numerically did not show decreasing skin friction with increasing loading. With increasing top load, the lateral load and displacements increased, showing a different behavior than that of the experimental data.
- The experimental mobilization of tip resistance of the piles was generally a function of the load level or the level of settlement of the pile, showing the need for considerable displacements for mobilization. The same behavior was shown by the numerical analysis, but the tip load obtained from the numerical analysis for the defective pile was higher than that obtained for the intact pile.
- Strain gauges were adequate for determining the loads on the top and tip of the piles, acquiring information on the load transfer. This information is considered essential to understanding the overall pile behavior.
- Defects in the piles manifest as a function of the load magnitude; therefore, it is suggested that an integrity evaluation of the piles should be performed soon after installing the piles because at this time, the piles are not yet subjected to loading from the superstructure. If necessary, the foundation can be reinforced by either changing the block geometry or installing new piles to minimize the impact on construction progress. This evaluation may be performed using the integrity test (PIT) and can be subsequently complemented with static load tests and dynamic loading tests, as recommended by the standard NBR 6122 (ABNT/2010).

Acknowledgments

The authors thank the São Paulo Research Foundation (Fundação de Amparo à Pesquisa no Estado de São Paulo – FAPESP), the National Council for Scientific and Technological Development (Conselho Nacional de Desenvolvimento Científico e Tecnológico - CNPq) and the Foundation for Research and Extension Support (Fundação de Apoio ao Ensino, Pesquisa e Extensão – FAEPEX - Unicamp) for the financial support necessary for research development. The authors also thank the Dywidag company for donating the rods used in the tests.

References

Abdrabbo, F.M. (1997). Misuse of soils and foundation causes disaster. Proc. Int. Conf. on Foundation Failures, Singapore, p. 121-130.

ABNT – Associação Brasileira de Normas Técnicas (2006). NBR 12.131: Estacas – Prova de Carga Estática. Rio de Janeiro, Brazil, 8 p.

ABNT – Associação Brasileira de Normas Técnicas (2010). NBR 6122: Projeto e Execução de Fundações. Rio de Janeiro, Brazil, 91 p.

Albuquerque, P.J.R. (2001). Estacas Escavadas, Hélice Contínua e Ômega Estudo do Comportamento à Compressão em Solo Residual de Diabásio, Através de Provas de Carga Instrumentadas em Profundidade. Tese de Doutorado em Engenharia, Escola Politécnica, Universidade de São Paulo, São Paulo, 272 p.

BSI – The British Standard Institution (2015). BS 8004: Code of Practice for Foundations. London, United Kingdom, 115 p.

Chung, D.N.; Kim, D. & Jo, S. (2010). Settlement of piled rafts with different pile arrangement schemes via centrifuge tests. Journal of Geotechnical and Geoenvironmental Engineering, 139(10):1690-1698.

Cordeiro, A.F. (2007). Avaliação Numérica de Reforço de Grupo de Estacas pela Introdução de Estacas Adicionais. Dissertação de Mestrado, Publicação G. Dm-155/07, Departamento de Engenharia Civil e Ambiental, Universidade de Brasília, Brasília, 118 p.

Cunha, R.P.; Cordeiro, A.F.; Sales, M.M. & Small, J.C. (2007). Parametric analyses of pile groups with defective piles: Observed numerical behaviour and remediation. Proc. 10th Australia - New Zealand Conference on Geomechanics, Brisbane, v. 1, pp. 454-459.

Cunha, R.P.; Cordeiro, A.F.B. & Sales, M.M. (2010). Numerical assessment of an imperfect pile group with defective pile both at initial and reinforced conditions. Soils and Rocks, 33(2):81-93.

Décourt, L. (1993). Predicted and measured behavior of non-displacement piles in residual soils. Proc. of BAP II, Deep Foundations on Bored and Auger Piles, Ghent, pp. 369-376.

Décourt, L. (1995). On the load-settlement behavior of piles. III Conferência Odair Grillo. Solos e Rochas, 18(2):93-112.

Freitas Neto, O.; Cunha, R.P.; Santos Júnior, O.F.; Albuquerque, P.J.R. & Garcia J.R. (2013). Comparison of numerical methods for piled raft foundations. Advanced Materials Research (Online), 838-841:334-341.

Freitas Neto, O. (2013). Avaliação Experimental e Numérica de Radiers Estaqueados com Estacas Defeituosas em Solo Tropical do Brasil. Tese de Doutorado, Publicação G.TD-088/2013, Departamento de Engenharia Civil e Ambiental, Universidade de Brasília, Brasília, 253 p.

Garcia, J.R. (2015). Análise Experimental e Numérica de Radiers Estaqueados Executados em Solo da Região de Campinas/SP. Tese de Doutorado, Faculdade de Engenharia Civil, Arquitetura e Urbanismo da Universidade Estadual de Campinas, Campinas, 359 p.

Gon, F.S. (2011). Caracterização Geotécnica Através de Ensaios de Laboratório de um Solo de Diabásio da Região de Campinas/SP. Dissertação de Mestrado, Faculdade de Engenharia Civil, Arquitetura e Urbanismo da Universidade Estadual de Campinas, Campinas, 153 p.

Klingmüller, O. & Kirsch, F. (2004). A Quality and safety issue for cast-in-place: 25 years of experience with low-strain integrity testing in Germany – From scientific peculiarity today-today practice. Proc. Current Practices and future trends in deep foundations, ASCE, Geotechnical Special Publication, Reston, n. 125, p. 202-221.

Kong, L. & Zhang, L. (2004). Lateral or torsional failure modes in vertically loaded defective pile groups. Journal Geotechnical Special Publication, 124:625-636.

Leung, Y.F.; Klar, A. & Soga, K. (2010). Theoretical study on pile length optimization of pile groups and piled rafts. Journal of Geotechnical and Geoenvironmental Engineering. ASCE. 136(2):319-330.

Makarchian, M. & Poulos, H.G. (1994). Underpinning by piles: a numerical Study. Proc. 13th International Conference on Soil Mechanics and Foundation Engineering, New Delhi, v. 4, pp. 1467-1470.

Novak, J.L.; Reese, L.C. & Wang, S.T. (2005). Analysis of Pile-Raft Foundations with 3D Finite-Element Method. Proceedings of the Structures Congress, New York, pp. 12.

Omeman, Z.M. (2012). Load Sharing of Piled-Raft Foundations in Sand Subjected to Vertical Loads. Ph.D. Thesis in the Department of Building, Civil and Environmental Concordia University. Montreal, Quebec, 131 p.

Petek, K.; Felice, C.W. & Holtz, R.D. (2002). Capacity analysis of drilled shafts with defects. Deep Foundations, Geot. Spec. Pub. ASCE, 2(116):1120-1135.

Poulos, H.G. (1997). Behaviour of pile groups with defective piles. Proc. 14th Int. Conf. Soil Mechanics Foundation Engineering, Hamburg, pp. 871-876.

Poulos, H.G. (2005). Pile behavior – Consequences of geological and construction imperfections. J. Geotech. and Geoenvir. Eng., ASCE, 131(5):538-563.

Prakoso, W.A. & Kulhawy, F.H. (2001). Contribution to piled raft foundation design. Journal of Geotechnical and Geoenvironmental Engineering, 127(1):17-24.

Rodriguez, T.G. (2013). Caracterização Geotécnica de um Solo de Diabásio por Meio de Ensaios SPT e CPT. Dissertação de Mestrado, Faculdade de Engenharia Civil, Arquitetura e Urbanismo da Universidade Estadual de Campinas, Campinas, 134 p.

Scallet, M.M. (2011). Comportamento de Estacas Escavadas de Pequeno Diâmetro em Solo Laterítico e Colapsível da Região de Campinas/SP. Dissertação de Mestrado, Faculdade de Engenharia Civil, Arquitetura e Urbanismo da Universidade Estadual de Campinas, Campinas, 166 p.

Schulze, T. (2013). Análise da Capacidade de Carga de Estaca Escavada Instrumentada de Pequeno Diâmetro por Meio de Métodos Semi Empíricos. Dissertação de Mestrado, Faculdade de Engenharia Civil, Arquitetura e Urbanismo da Universidade Estadual de Campinas, Campinas, 136 p.

Xu, K. (2000). General Analysis of Pile Foundations and Application to Defective Piles. Ph.D. Thesis, University of Sydney, 404 p.

Zhang, L. & Wong, E. (2007). Centrifuge modeling of large-diameter bored pile groups with defects. Journal of Geotechnical and Geoenvironmental Engineering ASCE, 133(9):1091-1101.

Zuquete, L.V. (1987). Análise Crítica da Cartografia Geotécnica e Proposta Metodológica para Condições Brasileiras. Tese de Doutorado, Escola de Engenharia de São Carlos, Universidade de São Paulo, São Carlos, 637 p.